Adsorption of Pure and Mixed Solvent Solutions of Spin Probes onto Stationary Phases

M. Francesca Ottaviani,* Michela Cangiotti, Giorgio Famiglini, and Achille Cappiello

Institute of Chemical Sciences, University of Urbino, Piazza Rinascimento, 6-61029, Urbino, Italy

Received: November 10, 2005; In Final Form: March 9, 2006

Water, methanol (MeOH), acetonitrile (ACN), and binary MeOH−water and ACN−water solutions of different spin probes (nitroxides), selected to mimic the behavior of different pollutants, were adsorbed onto stationary phases usually used in reversed-phase high-performance liquid chromatography (RP-HPLC). These stationary phases are constituted by porous silica and differ from each other regarding the surface area, the pore size, the particle size, the surface functions (NH_2, C8, and C18), and the percentage of functionalization. The electron paramagnetic resonance (EPR) spectra of the probe solutions adsorbed into the pores were analyzed by computer-aided computation of the spectral line shape, which provided structural and dynamical parameters of the probes and their environments. These parameters provided information on the surface properties of the stationary phases, such as alkyl chain density, solvent penetration, stationary-phase ordering, and residual silanol effects, which modify the retention times in HPLC. A different availability of polar surface groups in the pure and mixed solvents was found for the different stationary phases depending on (1) the different functionalization degree, (2) the surface-chain length, (3) the particle size, and (4) the polarity of both the probe and the solvent. The C8 functionalization rendered the surface more hydrophobic with respect to C18. The endcapping process of the residual silanols strongly enhanced the surface hydrophobicity tested by the probes. At the highest water content, the adsorption of the polar or charged probes onto the hydrophobic surface is the lowest and self-aggregation occurs. When the probes bear both hydrophilic and hydrophobic moieties, the adsorption is enhanced by a synergy between hydrophilic and hydrophobic bonds with the surface. A balance between the hydrophilic and hydrophobic forces leads to high adsorption and partial insertion of the surfactant probes in an ordered C18 chain layer at the solid surface which forms in the binary mixtures; this layer is ascertained between 40% and 70% of the less hydrophilic solvent, depending on the type of both the solid and the probe. This insertion and the response on the formation of the ordered layer were favored in ACN−water with respect to MeOH−water.

Introduction

The surface properties of the alkyl-functionalized stationary phases usually used in reversed-phase high-performance liquid chromatography (RP-HPLC) are a very debated matter. The importance of stationary-phase characteristics such as alkyl chain density, solvent penetration, stationary-phase ordering, and residual silanol effects on stationary-phase properties was carefully investigated, mainly by spectroscopic studies.[1−8] A critical point is the adsorption ability of the surface toward pollutants of different structure and polarity. This ability modifies the retention times and elution properties of the HPLC columns filled with stationary phases supported by the surface of small silica particles (3 and 5 μm particle size). Of course, the solvent polarity plays a crucial role in modifying the adsorption capability of the solid surface. Binary solvent solutions such as those used in gradient elution create particular effects onto the adsorption properties of the stationary-phase surface because of solvent microheterogeneity, solvent layering, and solvent-induced structural changes of the surface itself. Because of their importance as chromatographic eluents, mainly acetonitrile (ACN)−water and methanol (MeOH)−water solutions were used to elute through the stationary phases. Evidences of a microheterogeneous structure of such binary solutions were found in chromatographic systems,[9] for instance, separating water-rich and ACN-rich regions. This separation has also been proved theoretically.[10−12] In these conditions, the stationary phase, where the silica surface is functionalized with long alkyl chains, gave rise to an ordered structure. Fluorescence,[4,5] NMR,[6] and Raman[7,8] experiments have shown that mixed water−organic solvents favor a transition of the bonded alkyl chains from a collapsed layer to an extended one. Similar results were recently obtained by Henry et al. for a CD_3CN-D_2O solution in elution of model reversed-phase chromatographic interfaces by means of sum-frequency generation spectroscopy.[13]

Therefore, the structure of the liquid/solid interphase and the interacting ability of the surface of the stationary phase is a controversial problem which needs to be deeply studied. The electron paramagnetic resonance (EPR) technique provides a useful method of investigation of the surface properties of silica solids and of silica solid/liquid interphases.[14−18] When spin probes are introduced in specific sites of the system, depending on structure, polarity, and mobility, the computer-aided analysis of the EPR spectra reports on the interacting ability of the surface sites.[14−17] In the present study, we make use of different spin probes, selected to mimic the interacting properties of different pollutants toward the surface interacting sites, to investigate the interphase properties of stationary phases. Different commercial stationary phases commonly used in HPLC were first analyzed (from Nucleosil, Alltech (Adsorbosphere and Allsphere), and Water Spherisorb; see Table 1),

* To whom correspondence should be addressed. E-mail: ottaviani@uniurb.it. Tel: +39-0722-303319. Fax: +39-0722-303311.

10.1021/jp056516s CCC: $33.50
Published on Web 05/09/2006

TABLE 1: Names and Main Properties (as provided by the Trademarks) of the Stationary Phases Investigated in the Present Study

mark	pore size	particle size (μm)	surface area (m^2/g)	surface functions	covering %	acronym
Nucleosil	100 Å	5	350	C18	14	NC18
Nucleosil	100 Å	3	350	C18	14	N3C18
Alltech Adsorbosphere	80 Å	5	200	NH_2	12	ANH_2
Alltech Allsphere	80 Å	5	220	C18	6	AC18
Alltech Allsphere	80 Å	5	220	C18 endcapped[a]	>6	AC18E
Water Phase Sep Spherisorb	80 Å	5	220	C18	6	WC18
Water Phase Sep Spherisorb	80 Å	5	220	C8	n.d.	WC8

[a] The endcapping process is usually performed to render the residual SiOH groups hydrophobic. This process is currently achieved with small molecules able to approach the silanol groups, such as 3-methyl chlorosilane which forms the $Si-O-Si(CH_3)_3$ function.

SCHEME 1: Formulas of the Probes

CATn:

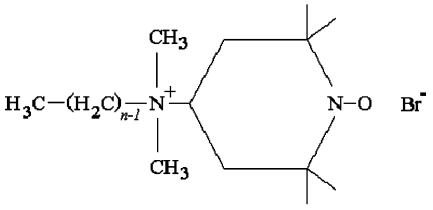

5DSA

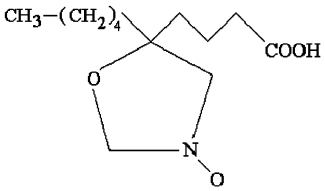

Py-T:

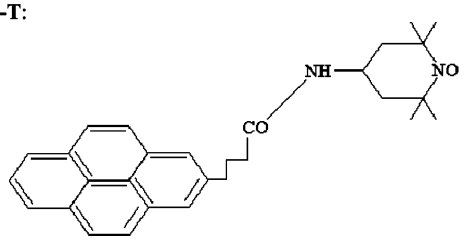

differing by the pore size, the particle size, the surface functionalization and its percentage, and the surface area. In the table, the different acronyms, used thereafter in the paper for the different stationary phases, are also indicated. A first analysis was performed by analyzing the adsorption properties of the solids toward the different probes from water solutions. Then, on the basis of this first analysis, we selected the two Nucleosil stationary phases at different particle sizes to analyze the structural variation played at the interphase by binary solutions (acetonitrile/water and methanol/water) of the same probes.

Experimental Section

The stationary phases were purchased from the various Trademarks, as indicated in Table 1. The surface properties provided by the manufacturers, that is, the pore size, the particle size, the surface area, and the surface functions and their covering percentage are also indicated in Table 1. The last column of the table lists the acronyms used for the various solids in this paper.

The radicals used as probes are shown in Scheme 1: (1) (top) 4-C1, 4-C9-, and 4C16-dimethylammonium-2,2,6,6-tetramethyl-piperidine-1-oxyl bromide (termed CAT1, CAT9, CAT16, respectively, and generally termed CAT*n*) which mimic the behavior of positively charged organic pollutants and cationic surfactants and investigate the effect played by the contemporaneous presence of hydrophilic and hydrophobic moieties in the pollutant materials; (2) (middle) 5-doxylstearic acid (5DSA), which mimics the adsorption of neutral surfactants; (3) (bottom) pyrene-$(CH_2)_3$-tempamide (Py-T), which reports on the adsorption of IPA molecules.

CAT1 and 5DSA were purchased from Sigma-Aldrich and used as received. CAT9, CAT16, and Py-T were kindly provided by Dr. X. Lei (Columbia University, NY).

We also used Tempo and Tempol probes (piperidine−nitroxide radicals with a proton and an OH group, respectively, as 4-substituents), which interacted poorly with the surface since they were slightly binding with both the hydrophilic and hydrophobic sites. Therefore, these probes were not able to monitor the surface properties of the stationary phases. Consequently, the results obtained with these probes are not henceforth described in this paper.

CAT*n* were solved in Millipore doubly distilled water, whereas 5DSA and Py-T were solved in chloroform (Merck) to get a 1 mM solution. Aliquots of 1 mL of the CAT*n* water solution were shaken with 125 mg of each stationary phase. Equivalent amounts (1 mL) of 5DSA and Py-T solutions in $CHCl_3$ were evaporated in vials. An amount of 1 mL of Millipore doubly distilled water was added to these vials and stirred with 125 mg of the solids. These water/solid mixtures in closed vials were left to equilibrate overnight in a dark and temperature controlled (20 °C) place. Samples were also prepared at lower radical concentrations (0.5, 0.1, 0.05, and 0.01 mM). After the equilibration, the solids were filtered, gently dried on a filter paper, and finally inserted in a 2 mm glass tube for the EPR analysis: these samples were termed *dry solids*. The wet solids, that is, the ones obtained after filtration without drying onto the filter paper, very often gave rise to a signal arising from free unadsorbed probes that cover the signal due to the probes at the solid surface. Therefore, the results from the wet solids are not informative regarding the surface properties and are not henceforth discussed in this paper. To determine the adsorbed amounts of radicals, the intensity decrease of the EPR signal from the unadsorbed radical solution to the supernatant solution after adsorption was analyzed by means of a flat cell fixed in the EPR cavity.

An equivalent procedure as described for the preparation of samples using water solutions of the probes was performed for mixed water−MeOH (Merck) and water−ACN (Merck) solutions, where the relative amounts of methanol and ACN were varied from 0% to 100%.

Other samples were prepared by packing the stationary phases in Teflon columns of 75 μm. Control tests were performed by HPLC by means of the injection of a resorcinol/naphthalene/anthracene solution in water/ACN = 45/55 and of a toluene/benzene/acetophenone solution in water/MeOH = 40/60. When the columns showed a good performance, solutions of the different nitroxides in the various solvents (pure water, MeOH,

ACN, and mixed water−MeOH and water−ACN, in isocratic conditions) were injected. After equilibration, pieces of each Teflon column were collected into a 4 mm glass tube and analyzed by EPR. However, in these cases, the analysis of the EPR spectra was poorly informative about the interacting ability of the surface, since the external solution was not removed and contributed in the wet and dry conditions to masking the component from the solution adsorbed into the pores. However, these components, obtained by subtracting the spectrum of the external solution, were equivalent to the EPR spectra recorded from the dry solids: this demonstrated the validity of the information from the EPR analysis of the dry solids, to be used by the HPLC applicants. For these reasons, this paper only presents and discusses the EPR results from the dry solids.

HPLC measurements were performed by means of a HPLC PUMP 420/422 KONTRON INSTRUMENTS.

EPR spectra were recorded by means of a EMX-Bruker spectrometer operating at X band (9.5 GHz) and interfaced with a PC (software from Bruker for the handling and analysis of the EPR spectra). The temperature was controlled with a Bruker ST3000 variable-temperature assembly cooled with liquid nitrogen.

Analysis of the EPR Spectra. The EPR spectra of the probes in unadsorbed solutions were constituted by three hyperfine lines (due to the coupling between the electron spin and the nuclear spin, the nuclear spin of the nitrogen atom, $I_N = 1$, generates $2I_N + 1 = 3$ lines) at almost the same intensities and a peak-to-peak distance corresponding to the isotropic hyperfine coupling constant $\langle A \rangle$. An increase in the environmental polarity of the NO group provokes an increase in the $\langle A \rangle$ value, due to the increased electron spin density on the nitrogen nucleus. The spectrum is centered at a magnetic field value which, at the fixed X-band frequency, corresponds to an isotropic g factor of about 2.006 (the g factor measures the coupling between the unpaired electron spin and the magnetic field). The relaxation mechanism of the nitroxides is due to the modulation of the **A** and **g** tensor components generated by the rotational diffusion motion of the probes. When the probes link the surface sites, their rotational mobility is hindered and the peaks due to the anisotropic components of the **A** and **g** tensors start resolving. Indeed, the main parameter which monitors the occurring interactions of the probes with the surface is the correlation time for the rotational diffusion motion around the NO direction, which is perpendicular to the direction of the p orbital containing the unpaired electron (τ_{perp}). A Brownian diffusion motion was assumed, for which the diffusion component $D_{perp} = 1/(6\tau_{perp})$. This parameter was extracted from the computer-aided analysis of the spectral line shape, performed by means of the well-established procedure of Budil and Freed.[19] Therefore, τ_{perp} significantly increases when the probes are bonding with surface groups. The computation also needs as input parameters the main **g** and **A** tensor components. The **g** anisotropy is usually small for nitroxide radicals and is well reproduced by assuming constant main g_{ii} components ($g_{xx} = 2.009$, $g_{yy} = 2.006$, and $g_{zz} = 2.002$), as already assumed in previous studies for similar systems. Small variations of these components poorly affected the EPR line shape, due to the usual broadening of the lines in open-air (oxygenated) systems.

The hyperfine coupling components A_{ii} also changed from one system to another system, monitoring the variation in the environmental polarity of the probes and, eventually, the anisotropy of the coupling.

When the radicals are close to one another, spin−spin interactions led to line broadening and eventually to the collapse of the three hyperfine lines. In this case, the increase in the intrinsic line width ($W1$) from the usual $W1 = 1 - 2$ G value monitored the occurrence of spin−spin interactions.

When the chains of the surfactant probes insert in the packed chains attached at the solid surface, an order parameter, S, was added in the calculation (in a correspondent Hamiltonian component) to evaluate the wobbling motion of the chains in the chain layer. An increase in the order parameter ($0 < S < 1$) corresponds to an increased organization of the layer toward a packed structure characterized by the carbon chains parallel to one other, and a decrease in S corresponds to a more loose packing of the lipid layer where the chains oscillate and twist to and from one other.

Four different signals, due to probes in different environmental conditions, may contribute to the experimental spectra (usually two or, as a maximum, three signals contemporaneously) and are separated from one other by subtraction of experimental spectra. These signals differ from one another depending on the main parameters which characterize the computation, as follows:

(a) *Free signal*, due to noninteracting free probes, characterized by a low τ_{perp} value. To compute this signal, we vary the A_{ii} and τ_{perp} input parameters.

(b) *Interacting signal*, due to single probes linked to surface polar sites (silanol groups), characterized by a high τ_{perp} value. To compute this signal, we vary the A_{ii} and τ_{perp} input parameters.

(c) *Aggregating signal*, due to probes linked to close surface sites characterized by large line-broadening (high W1). To compute this signal, we vary the $W1$ parameter, whereas A_{ii} and τ_{perp} are considered constant ($A_{ii} = 7$ G, 7 G, 35 G; $\tau_{perp} = 8$ ns) since their variations poorly affect the line shape of such broadened signals.

(d) *Ordered signal*, due to probes inserted in an ordered layer, characterized by an order parameter S. To compute this signal, we vary S, A_{ii}, and τ_{perp} input parameters.

We have to consider the following:

(i) The starting input parameters were chosen by comparing the experimental signals with the several spectral computations already performed for similar systems.

(ii) The variation of each parameter produces well distinguishable variations in the EPR line shape. For instance, a high S value produces unique spectral features (narrow peaks beside the central lines). Therefore, the occurrence of the ordering effect and its variation are well distinguished from the effects due to the other parameters in the spectral computation.

(iii) Of course, a different selection of parameters may produce an equivalent or even better fit between the experimental and the computed line shapes, but the goal was to obtain information by varying only one or two parameters in a series of spectra of similar or equivalent systems, by also comparing with the parameters previously obtained for similar systems.

The subtraction of spectra from one another provided each signal (for instance, subtracting a spectrum constituted of signal (a) from a spectrum constituted by both signals (a) and (b) allows us to extract the two signals, (a) and (b)). Apparent fine structure and noise may appear due to the subtraction procedure. Then, the computation of each signal was performed. Double integration of each signal gives the relative percentages of the probes in the different environmental conditions. Finally, the EPR experimental spectra were reproduced by adding the computed signals at their relative intensities (relative percentages of the probes).

TABLE 2: Relative Percentage of the Interacting Signal for the Various Probes (1 mM in water solutions) Adsorbed onto the Different Stationary Phases (dry solids)[a]

sample	CAT1	CAT9	CAT16	5DSA	Py-T
NC18	0 (5)[b]	15 (10)	65 (80)	100 (90)	90 (95)
N3C18	0 (5)	10 (10)	65 (80)	100 (90)	90 (95)
ANH_2	90 (50)	75 (40)	70 (90)	0 (5)	15 (15)
AC18	90 (5)	95 (40)	100 (90)	100 (85)	100 (80)
AC18E	0 (5)	0 (10)	60 (75)	100 (90)	90 (100)
WC18	25 (5)	35 (15)	70 (85)	100 (90)	100 (90)
WC8	0 (5)	0 (5)	0 (80)	100 (90)	85 (95)

[a] The remaining percentage, not reported, was due to the free and/or the aggregating signals. [b] In parentheses, the percentage of adsorbed solution is reported.

The accuracy of the parameters extracted from computation was 2%.

Results and Discussion

Adsorption of the Probes onto the Different Phases from Water Solutions. The analysis of the results is initially described and discussed for each probe, then a comparison among the probes was performed to underline the main effects onto the probe−surface interactions on the basis of the structural and polarity variations of the probes themselves.

As described in the Experimental Section, two kinds of samples were inspected by EPR:

(1) After equilibration of the radical solution with the solid, the amount of adsorbed species was calculated (in percentage) by evaluating the intensity decrease of the EPR spectra from the unadsorbed solution to the supernatant solution after adsorption. This is discussed in terms of "*adsorbed solution*".

(2) EPR spectra were recorded and analyzed for the filtered solid gently dried onto a filter paper to remove the external solution. In this case, the remaining probes are those internalized in the pore structure still retaining the solvent. These samples were henceforth termed "*dry solids*".

CAT1. *Adsorbed Solution*. As reported in parentheses in Table 2, only ∼5% of the radical solution was adsorbed at the hydrophobic silica surfaces, whereas the adsorption onto ANH_2 was about 50%: as expected for a positively charged molecule, its adsorption onto a surface is modulated by the surface polarity and potential.

Dry Solids. With the exception of the ANH_2 sample, the EPR spectra were constituted mainly by the free signal, since CAT1 was repulsed by the hydrophobic surface. But, the hydrophobic stationary phases also adsorbed the probes at the polar groups which survived after the grafting procedure, giving rise to an interacting signal. Therefore, the EPR spectra were constituted by two signals: the interacting and the free ones.

Figure 1a shows the experimental spectrum (298 K) obtained for CAT1 adsorbed onto WC18: the free signal (dashed line) is equivalent to that obtained for unadsorbed CAT1 solutions ($\tau_{perp} \sim 0.1$ ns). This signal was subtracted from the experimental WC18−CAT1 spectrum to extract the interacting signal (dotted line). This interacting signal did not modify from one another CAT1 dry solids, and it was computed as shown in Figure 1b (full line, experimental spectrum; dashed line, computed spectrum), by means of the main parameters (A_{ii} and τ_{perp}) reported in the figure. The A_{ii} values are in line with a polar environment of the radicals, sitting at polar surface sites (mainly silanols); the low mobility (relatively high τ_{perp}) demonstrated the interactions occurring between these sites and the charged probes.

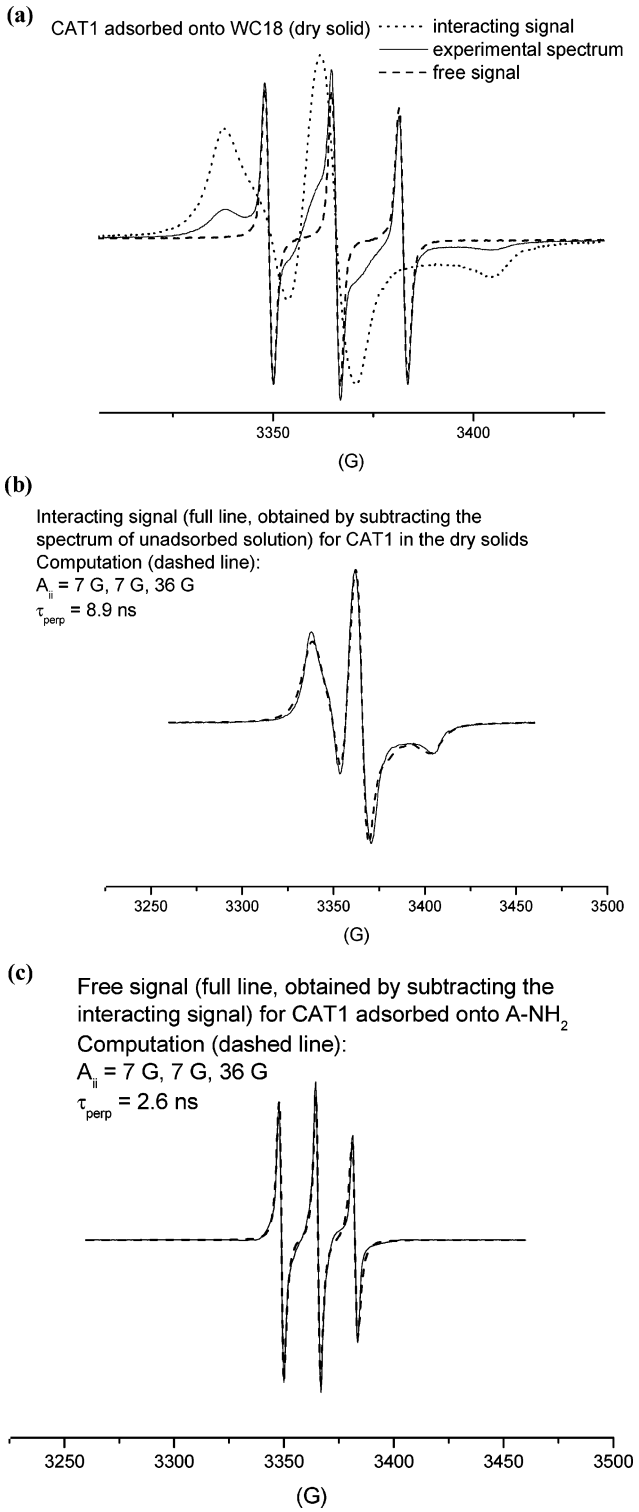

Figure 1. (a) Experimental EPR spectrum (298 K) obtained from CAT1 (1 mM in water solution) adsorbed onto WC18: subtraction of experimental spectra allowed us to extract the two signals, the interacting one (dotted line) and the free one (dashed line). (b) Experimental (full line) and computed (dashed line) interacting signals of CAT1 (1 mM in water solution) binding the stationary-phase surface; the main parameters obtained from computation (A_{ii} and τ_{perp}) are also reported in the figure. (c) Experimental (full line) and computed (dashed line) free signals of CAT1 adsorbed onto ANH_2; the main parameters obtained from computation (A_{ii} and τ_{perp}) are also reported in the figure.

CAT1 adsorbed onto ANH_2 is mainly interacting with the surface (interacting signal the same as that in Figure 1b). The free signal (10%), obtained by subtracting the interacting signal

in Figure 1b from the experimental ANH_2−CAT1 spectrum, is shown in Figure 1c: the computation (dashed line in Figure 1c) was performed by means of a τ_{perp} at the border between fast and slow tumbling of the radicals. This indicates that these "free" CAT1 probes, even if not directly interacting with the ANH_2 surface groups, are still affected by the surface potential and their rotational mobility is consequently partially hindered, as already found for hydrophilic silica surfaces.[14−18]

The different percentages of the interacting signal were evaluated for the different hydrophobic stationary phases. This amount nicely works as a proof of the quality of the grafting procedure. The percentages of the interacting signal are reported in Table 2 for the various stationary phases. The dry, solid WC18 shows a consistent fraction of interacting signal (about 25%), which indicates a relatively low hydrophobicity of the surface. In line with a larger C18 surface covering (Table 1), NC18 showed 0% of the interacting signal. Unexpectedly (on the basis of the same surface covering and the same amount of adsorbed solution as WC18), the AC18 surface was significantly interactive (90% of interacting signal) with CAT1: this indicated that the residual silanol surface groups at the AC18 surface are well available to CAT1 interaction. But, the endcapping process, leading to the AC18E sample, strongly increases the hydrophobicity of the surface, thus preventing its interaction with the charged probe.

CAT9. *Adsorbed Solution*. As reported in parentheses in Table 2, the adsorption of CAT9 increases with respect to CAT1. About 10−15% of the probes were adsorbed onto the hydrophobically functionalized stationary phases, with the exception of AC18, which adsorbs about 40% of the probes, and WC8, for which the adsorption is very low (5%). For ANH_2 (40% adsorption), CAT9 is less adsorbed than CAT1. All these results are easily explained considering the higher hydrophobicity of CAT9 with respect to CAT1 and the possibility to insert the surfactant probe chain in the chains attached to the surface.

Dry Solids. The higher CAT9 hydrophobicity was responsible for the increased percentage of the interacting signal for the adsorbed radicals onto NC18 and N3C18 (N3C18 adsorbed less than NC18) but, mainly, onto AC18 and WC18, as shown in Table 1. This indicates that the charged CAT group easily accedes to the polar surface sites, due to synergic hydrophilic and hydrophobic interactions between CAT9 and the solid surface. Accordingly, the rotational mobility of the interacting CAT9 probes decreased (increase of τ_{perp}) with respect to CAT1, as obtained by computing the interacting signal (Figure 2a). Furthermore, an aggregating signal contributed to the EPR spectrum, due to self-aggregation of the radicals in the pore structure, favored by condensation of the radical chains around the surface carbon chains. The largest percentage of the aggregating signal (about 50%) was found for WC18. Figure 2b shows the experimental spectrum (full line; 298 K) and the computed signals (dashed line, aggregating signal; dotted line, interacting signal; dashed−dotted line, free signal) for CAT9 (1 mM in water solution) adsorbed onto WC18. The aggregating signal was obtained by subtracting the interacting signal shown in Figure 2a, and a small percentage (8−10%) of the free signal was obtained from the unadsorbed solution and computed with A_{ii} = 7 G, 7 G, 34 G and τ_{perp} = 0.5 ns. This aggregating signal was computed by increasing the line width ($W1$) to 20 G (A_{ii} = 7 G, 7 G, 35 G; τ_{perp} = 8 ns), consistent with condensed radicals at the surface.

Control EPR measurements, performed at lower CAT9 concentrations (results not shown), revealed a relative intensity decrease of the aggregating component with respect to the interacting component. At the lowest radical concentrations (at the limit of EPR sensitivity), only the interacting component remained. This means that the CAT9 heads occupy the available polar interacting groups at the solid surface, and then, after their saturation, self-aggregation occurs.

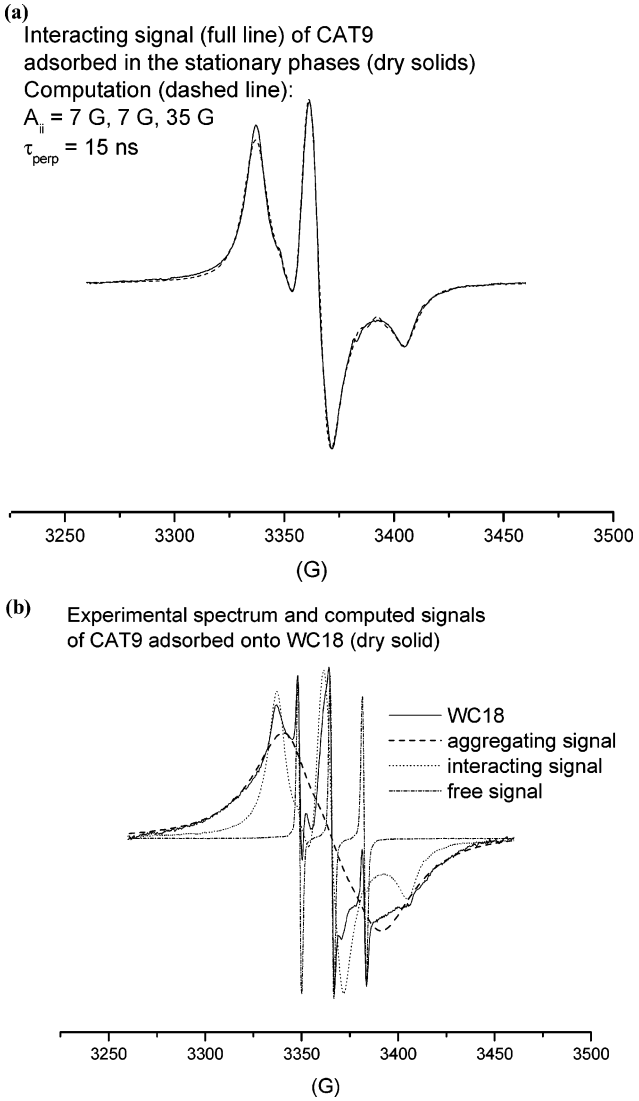

Figure 2. (a) Experimental (full line) and computed (dashed line) interacting signals for CAT9 (1 mM in water solution) binding the stationary-phase surface; the main parameters obtained from computation (A_{ii} and τ_{perp}) are also reported in the figure. (b) Experimental spectrum (full line, 298 K) and computed signals (dashed line, aggregating signal; dotted line, interacting signal; dashed−dotted line, free signal) for CAT9 (1 mM in water solution) adsorbed onto WC18.

CAT16. *Adsorbed Solution*. The adsorption of the solution is strongly enhanced with respect to CAT9, and the supernatant solutions after adsorption show a very weak spectrum for all the samples: the percentage of adsorbed solution is reported in parentheses in Table 2.

Dry Solids. With the exception of WC8, the high relative amounts of the interacting signal (Table 2) indicated that all the hydrophobic stationary phases interact well with this probe, due to an easy insertion of the radical chain among the C18 chains attached at the surface, while the charged CAT heads interact with the available polar surface sites. The remaining fraction of radicals, with respect to the interacting fraction, gave rise to an aggregating signal, and no free signal was evident in the EPR spectra of the dry solids.

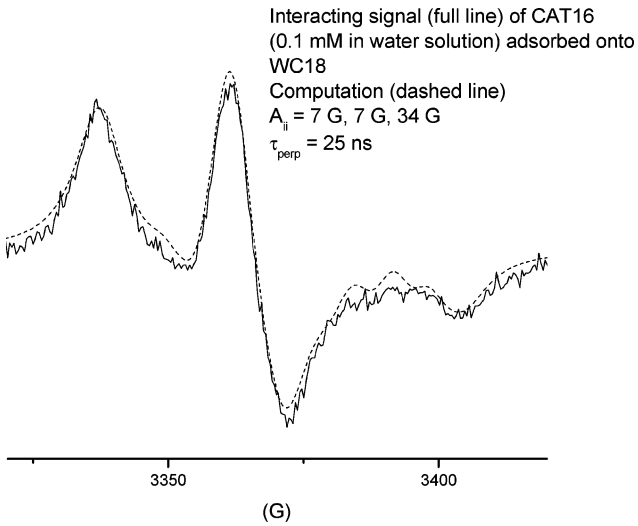

Figure 3. Experimental (full line) and computed (dashed line) interacting signals for CAT16 (0.1 mM in water solution) binding WC18; the main parameters obtained from computation (A_{ii} and τ_{perp}) are also reported in the figure.

Figure 3 shows the interacting signal obtained for 0.1 mM CAT16 adsorbed onto WC18. The A_{ii} corresponds to a "middle polarity" environment, which is identified in the radicals heads in the same vicinity of both silanols and C18 chains. When the CAT16 concentration is increased, these interacting sites saturate and other sites at different environmental polarity are occupied, giving rise to different spectral components (results not shown).

It is interesting to note that the rotational mobility of the interacting signal was lower for CAT16 with respect to CAT9. The stronger interaction of CAT16 with respect to CAT9 is due to an enhanced synergy between hydrophilic and hydrophobic interactions with the surface.

5DSA. *Adsorbed Solution*. The probe was largely adsorbed at the hydrophobicized silica surfaces and negligibly adsorbed onto ANH_2 (percentages reported in parentheses in Table 2).

Dry Solids. The spectrum obtained for the dry ANH_2 solid was constituted by the only free signal, whereas the other stationary phases only showed the interacting signal. The EPR spectra of 5DSA adsorbed onto the hydrophobic stationary phases were very similar to each other, characterized by $\tau_{perp} = 20$ ns and $A_{ii} = 7$ G, 7 G, 34 G, that is, equivalent to the interacting signal in Figure 3b.

Py-T. *Adsorbed Solution*. The probe was largely adsorbed at the hydrophobicized silica surfaces (total adsorption onto AC18E and relatively lower adsorption onto AC18) and poorly adsorbed onto ANH_2 (percentages reported in parentheses in Table 2).

Dry Solids. The spectrum obtained for the dry ANH_2 solid was only constituted by the free signal. For the other stationary phases, the spectra were mainly constituted by the interacting signal (percentages reported in Table 2).

The interacting signal was computed with different main parameters: for AC18, WC18, and WC18E, $\tau_{perp} = 10$ ns, $A_{ii} = 7$ G, 7 G, 36.5 G; for WC8, $\tau_{perp} = 8$ ns, $A_{ii} = 7$ G, 7 G, 35.5 G; for NC18 and N3C18, $\tau_{perp} = 5$ ns, $A_{ii} = 7$ G, 7 G, 37.5 G.

These parameters suggest the following behavior:

(a) The high A_{zz} parameters indicated a high environmental polarity of Py-T: the nitroxide group does not insert in the hydrophobic surface layer and probably retains the hydration layer.

TABLE 3: Percentage of Adsorbed Solution and Percentage of Interacting Signal in the Spectra of CAT1 in Mixed MeOH−Water and ACN−Water Solutions, Adsorbed onto NC18

solvent (%)	adsorbed solution (%)	interacting signal (%)
100−80 Me	33	80
70−50 Me	20	85
40−20 Me	15	50
10 Me	5	20
100−80 ACN	72	90
70−60 ACN	55	90
50−20 ACN	33	85
10 ACN	5	20

(b) In line with the above finding, the mobility tested by τ_{perp} is in general faster than that found for the other probes, despite the large size of the Py-T probe. However, it must be kept in mind that the linking between the pyrene and the Tempo moieties, via a $CH_2-CH_2-CH_2$ group, permits fast rotation of the Tempo unit.

(c) The WC8 sample has a more hydrophobic surface (better functionalized than the C18 phases), in agreement with the results from the other probes.

(d) The Nucleosil stationary phases show a lower retention of this kind of probe, which mimics the behavior of IPA pollutants well.

Adsorption of the Probes onto NC18 and N3C18 Phases from Mixed Water/Methanol and Water/ACN Solutions. On the basis of the results described in the previous section, we selected NC18 and N3C18 to analyze the structural variation played at the interphase by binary solutions (acetonitrile/water and methanol/water).

In this case too, we separately analyze the results from each probe.

CAT1. *Adsorbed Solution*. As reported in Table 3, the percentage of adsorbed solution increased with the increase in methanol or in ACN with respect to water: the more hydrophobic solvents favored the access of the charged radical to the hydrophobic surfaces.

N3C18 adsorbed less CAT1 than NC18. The largest percentage of adsorbed solution onto N3C18 is only 40% in pure ACN. This indicates a much higher hydrophobicity of the N3C18 surface with respect to the NC18 one.

Dry Solids. As also reported in Table 3, the increase in the relative contents of ACN and MeOH with respect to water favored the interactions between CAT1 and the polar surface sites, giving rise to an increasing percentage of the interacting signal ($\tau_{perp} = 7.5$ ns). This means that the access to the polar surface sites is favored at high methanol or ACN content. This effect is more significant for the ACN−water binary solvent with respect to the MeOH−water one. This is because the charged probes are repulsed by the hydrophobic solvent and by the hydrophobic surface chains and refuge to the surface polar sites. Furthermore, the conformation of the chains themselves creates "channels" that conduce the probes to the polar sites.

The percentage of the interacting component is much lower for N3C18 with respect to NC18 and aggregation occurs. Consequently, the intensity of the spectra of the dry N3C18 solid is very low and poorly informative. This is explained by considering a higher C18 functionalization (higher chain density) of the N3C18 surface with respect to the NC18 surface.

CAT9 and CAT16. The results of CAT9 and CAT16 are described and discussed together since the main information comes from the comparison of the results from these two probes.

TABLE 4: Percentage of Adsorbed Solution and Main Parameters (from computation) of the Signals Constituting the EPR Spectra of CAT9 and CAT16 Adsorbed onto NC18: % and τ_{Perp} (interacting signal); %, *S*, and τ_{Perp} (ordered signal); % and W1 (aggregating signal)

(a) Signals Constituting the EPR Spectra of CAT9

solvent (%)	adsorbed solution (%)	aggregating signal		interacting signal		ordered signal		
		(%)	*W*1 (G)	(%)	τ_{perp} (ns)	(%)	*S*	τ_{perp} (ns)
100−70 Me	25	0	0	100	16.6	0	0	0
60 Me	45	0	0	10	16.6	90	0.4	0.84
50 Me	69	0	0	5	16.6	95	0.18	0.86
40−30 Me	20	10	20	90	12.6	0	0	0
20−10 Me	20	50	20	50	18	0	0	0
100−80 ACN	35	0	0	100	16.6	0	0	0
70−60 ACN	50	0	0	100	16.6	0	0	0
50 ACN	72	0	0	15	12.6	85	0.42	0.68
40 ACN	95	0	0	10	12.6	90	0.42	0.68
20 ACN	98	0	0	5	12.6	95	0.42	0.68
10 ACN	40−20	40	20	60	19−18	0	0	0

(b) Three Signals Constituting the EPR Spectra of CAT16

solvent (%)	adsorbed solution (%)	aggregating signal		interacting signal		ordered signal		
		(%)	*W*1 (G)	(%)	τ_{perp} (ns)	(%)	*S*	τ_{perp} (ns)
100−60 Me	50	0	0	100	16.6	0	0	0
50−30 Me	5	0	0	100	16.6	0	0	0
20 Me	5	20	25	80	12.6	0	0	0
10 Me	20	35	25	65	18	0	0	0
100−70 ACN	40	0	0	100	16.6	0	0	0
60−30 ACN	50	0	0	25	16.6	75	0.44	0.98
20−10 ACN	20	30	20	70	20	0	0	0

Adsorbed Solution. As reported in Table 4a, the adsorbed amount of CAT9 was relatively low both in methanol or in ACN-rich solutions and in water-rich solution but significantly increased in mixed solvents (for 50% MeOH and, mainly, for 20−40% ACN). Conversely, as reported in Table 4b, CAT16 was more adsorbed from pure methanol solutions than from the mixed MeOH−water solvents, but the mixed ACN−water solutions at 30−60% ACN also gave an increase in the adsorbed solution. However, in all cases, CAT16 was less adsorbed than CAT9. The increase in adsorption is ascribed, as described below for the dry solids, to the insertion of the surfactant radical into the organized chains (in an ordered layer) at the stationary-phase surfaces. This organization is therefore favored in ACN−water mixed solvents, with respect to the MeOH−water mixed solvents, and CAT9 inserts better in the ordered layer than CAT16.

Dry Solids. At the lowest MeOH and ACN contents (10%), the spectra are constituted by the interacting and the aggregating signals (Table 4): in these conditions the amount of aggregating signal is lower in ACN than in MeOH and is lower for CAT16 than for CAT9. This is in line with an easier insertion of CAT16 into the C18 chains approaching the charged surfactant head to the polar surface sites, mainly in the presence of the more hydrophobic ACN solvent.

At higher ACN and MeOH content, the aggregating signal disappears and an ordered signal contributes to the EPR spectra. This ordered signal is characterized by the order parameter, due to the insertion of the surfactant probes in an ordered C18 layer at the stationary-phase surface. Figure 4 shows as examples the experimental (full line) and computed (dashed line) ordered signals (the computation procedure is described in the section about the Analysis of the EPR Spectra) for CAT9 (a) and CAT16 (b) at a concentration of 1 mM in water/ACN = 1:1 solution (dry NC18 solids); the main parameters obtained from computation (A_{ii}, *S*, and τ_{perp}) are also reported in the figures. As it results from Table 4, the ordered component becomes the main spectral component (85−95%) in the spectra of CAT9 at 40−50% of MeOH and at 20−50% of ACN, whereas it appears between 30% and 60% of ACN for CAT16. Therefore, CAT9 monitors the formation of the ordered C18 layer better than CAT16. This is because of a deep insertion of CAT16 in the C18 chains: the charged head interacts with the polar surface sites and probably the radical plays a perturbing role in the organization of the environmental chains. The ordering effect was more pronounced for the water−ACN mixtures than for water−MeOH ones; the water−MeOH mixtures show (1) a smaller percentage of the ordered component, (2) a smaller order parameter, (3) a larger amount of low polar solvent which is needed to create the ordering.

as an effect, CAT16 in the binary MeOH−water mixture does not show the stationary-phase ordering. The higher ordering effect of ACN with respect to MeOH is ascribed to a balance between hydrophilic and hydrophobic forces in stabilizing the palisade organization of the chains.

However, this structuring of the stationary surface chains is monitored only in a limited range of binary solvent compositions, since the ordered signal disappears above 70% of ACN or MeOH and only the interacting signal remains to contribute to the overall EPR line shape. It is interesting to note that the mobility of the probes interacting with the surface is higher when the ordering signal also contributes to the spectrum, that is, in the intermediate compositions of the binary solvents. This is in line with the insertion of the radicals among the ordered chains, which do not allow an easy interaction of the radical heads with the surface sites.

Therefore, the EPR analysis was able to describe the structural ordering of the stationary phase at the solid/liquid interphase occurring at particular binary solvent compositions.

Another piece of information is obtained by comparing the results of NC18 and N3C18, which only differ by particle size. N3C18 dry samples with 80% MeOH and 30% ACN show the same spectra as NC18 with 60% MeOH and 20% ACN, respectively. That is, the lower the particle size, the higher the amount of low polar solvent needed to monitor the ordered layer. Furthermore, the higher the water content, the higher the amount

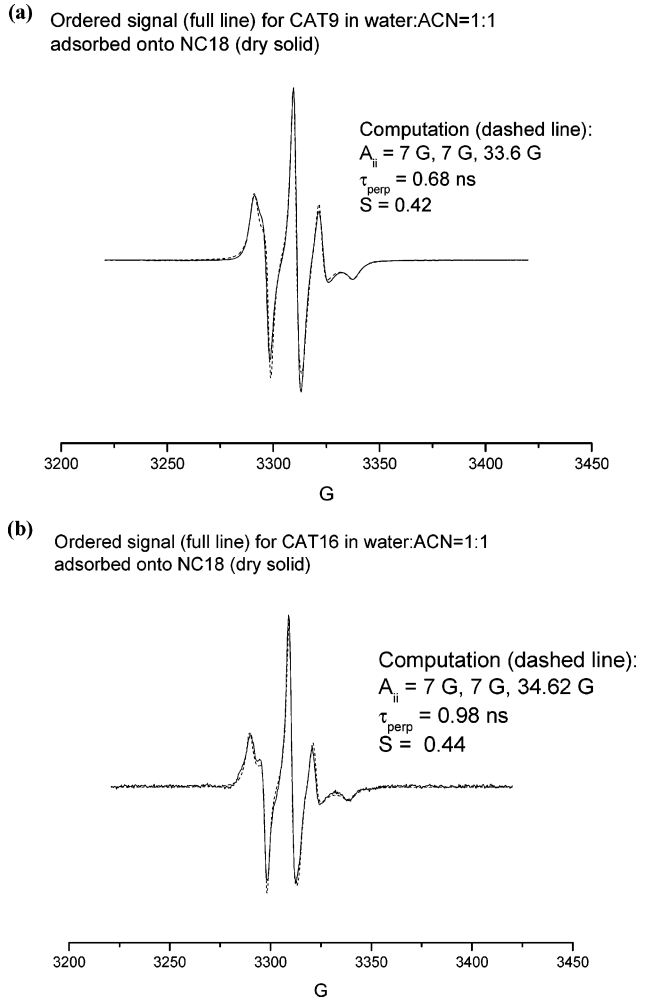

Figure 4. Experimental (full line) and computed (dashed line) ordered signals for CAT9 (a) and CAT16 (b) (1 mM in water/ACN = 1:1 solution) binding the stationary-phase NC18; the main parameters obtained from computation (A_{ii}, S, and τ_{perp}) are also reported in the figure.

of aggregating component of CAT9 in N3C18, in line with a higher density of C18 chains.

Indeed, CAT16 adsorbed onto N3C18 does not originate an ordered component at any binary mixture, due to a high covering of the N3C18 surface with C18 chain.

5DSA and Py-T. *Adsorbed Solutions*. In line with the trend showed by increasing the hydrophobicity from CAT9 to CAT16, the adsorption of 5DSA and Py-T onto the stationary phases is complete at any composition of the binary mixtures (no EPR signal is recordable in the supernatant solutions after adsorption).

Dry Solids. The spectra of the dry solids only show an interacting component (equivalent to that shown in Figure 3b for CAT16), due to the interaction of the nitroxide group with the polar surface groups, while the stearic chain or the Py moiety interacts with the C18 chains. Therefore, these probes do not report about the formation of the ordered C18 layer but indicate a high retention of these kind of molecules when adsorbed onto hydrophobic stationary phases using mixed eluting solvents. This kind of information is valuable for the use of these materials in HPLC.

Conclusions

The analysis of the EPR spectra of water solutions of different spin probes (CAT*n*, where $n = 1$, 9, and 16, 5DSA, and Py-T), selected to mimic the behavior of different pollutants, adsorbed

SCHEME 2: Proposed Organizations of the Positively Charged Probes at the C18 Stationary-Phase Surface at Which the Different Signals Originate: Free, Interacting, Aggregating, and Ordered

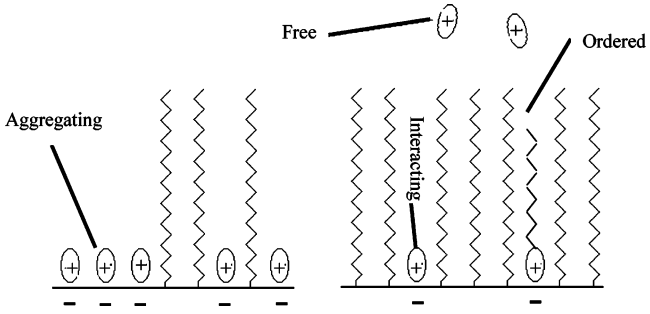

onto stationary phases of different Trademarks revealed a singular availability of polar surface sites, even if the silanol surface groups were functionalized with hydrophobic carbon chains. The highest covering of hydrophobic chains was found for WC8, whereas the solids bearing a C18 chain show a partial covering and only a partial hydrophobicity of the surface. For the different phases investigated in the present study, the availability of polar surface groups, as revealed by the EPR analysis, follows the trend: ANH_2 > AC18 > WC18 > NC18 > N3C18 > AC18E = WC8. Interestingly, AC18 interacted well with both low polar and high polar probes, whereas the endcapping process rendered AC18E completely hydrophobic. The surfactant probes partly self-aggregated in the water pools inside the pores but also well interacted with the solid surface due to contemporaneous hydrophilic and hydrophobic interactions with the polar surface sites and the C18 or C8 chains, respectively.

Therefore, the spin probe technique provided detailed information on the interacting ability of the various stationary-phase surfaces and on the different qualities of the chain functionalization, which is needed for the correct use of these phases in HPLC.

NC18 and N3C18 were selected to perform the analysis of the adsorption behavior of the surface when binary water−MeOH and water−ACN solutions were used at different relative percentages of the two solvents.

The main results are summarized in the following and sketched in Scheme 3:

(a) At the highest water content, the adsorbed solutions of the charged probes is very low, and self-aggregation occurs due to repulsion between the polar or charged nitroxide groups and the hydrophobic C18 surface. The longest chain probes interact better with the surface using both hydrophilic and hydrophobic interactions, as shown in Scheme 2a.

(b) At the highest MeOH or ACN contents, the adsorption is still low but higher than that in water. No self-aggregation of the probes was found, and the charged groups of the surfactants approach the polar surface groups, as shown in Scheme 2b for CAT9.

(c) For the mixed solvents, between 40 and 70% of MeOH or ACN, the adsorption is the maximum for all the probes. The C18 chains form an ordered layer at the surface, and an ordered signal contributes to the EPR spectra of the charged surfactant probes, since the CAT group approaches the polar surface groups and the surfactant chain inserts in the ordered layer. The adsorption modes of CAT9 and CAT16 are proposed in parts c and d of Scheme 3, respectively: CAT9 nicely testifies about the formation of the ordered C18 layer due to a balance between the hydrophilic and hydrophobic forces. On the contrary, the

SCHEME 3: Proposed Locations of the Probe Solutions at the Stationary-Phase Surfaces: (a) CAT1 and CAT16 in Water, (b) CAT9 in ACN, (c) CAT9 in MeOH−Water and ACN−Water, and (d) CAT16 in MeOH−Water and ACN−Water

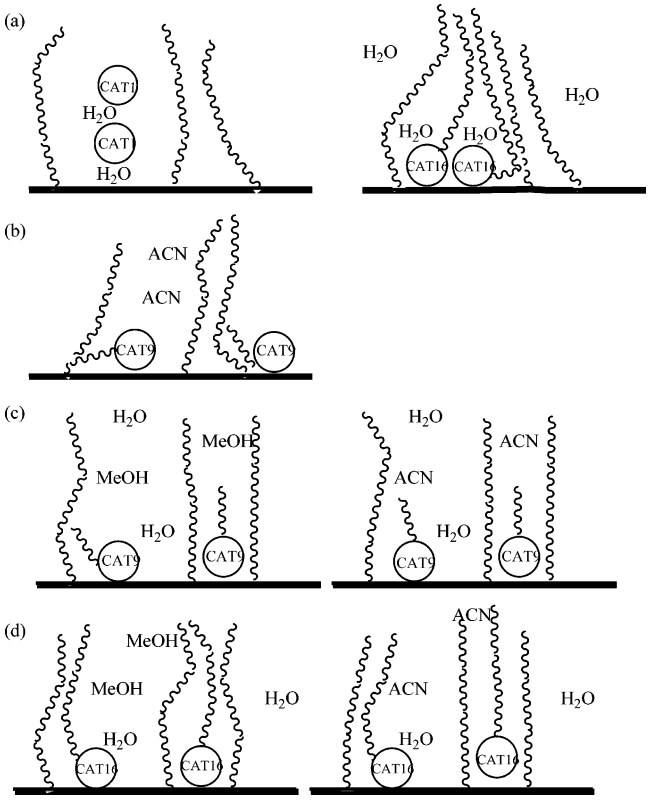

increased hydrophobicity of CAT16 and, more, of 5DSA, perturbs this balance and impedes checking of the ordering of the chains, mainly in mixed methanol solutions. The increasing hydrophobicity of the surfactant probe favors the interactions of the polar or charged nitroxide groups with the polar surface groups.

(d) Parts c and d of Scheme 2 also show that the ordering effect is more significant to the ACN−water mixed solvent with respect to MeOH−water.

(e) Finally, the EPR results indicate a higher density of C18 chains at the N3C18 (particle diameter of 3 μm) surface with respect to NC18 (particle diameter of 5 μm).

Definitely, these pieces of information are helpful to clarify the behavior of the stationary phases for HPLC, with respect to the retention of different pollutants, which is modulated by the structure of the stationary phase and the elution ability of the solvents.

Acknowledgment. M.F.O. and M.C. thank Maristella Martina and Emiliano Sartini for the great help in recording and analyzing the EPR spectra. The authors thank the Italian Ministry of University and Scientific Research (MURST) for financial support.

References and Notes

(1) DeVido, D. R.; Dorsey, J. G.; Chan, H. S.; Dill, K. A. *J. Phys. Chem.* **1998**, *102*, 7272.

(2) Alvarez-Zepeda, A.; Barman, B. N.; Martire, D. E. *Anal. Chem.* **1992**, *64*, 1978.

(3) Bliesner, J. M.; Sentell, K. B. *Anal. Chem.* **1993**, *65*, 1819.

(4) Carr, J. W.; Harris, J. M. *Anal. Chem.* **1987**, *59*, 2546.

(5) Burns, J. W.; Bialkowski, S. E.; Marshall, D. B. *Anal. Chem.* **1997**, *69*, 3861.

(6) Pursch, M.; Brindle, R.; Ellwanger, A.; Sander, L. C.; Bell, C. M.; Händel, H.; Albert, K. *Solid State Nucl. Magn. Reson.* **1997**, *9*, 1919.

(7) Thompson, W. R.; Pemberton, J. E. *Anal. Chem.* **1994**, *66*, 3362.

(8) Doyle, C. A.; Vickers, T. J.; Mann, C. K.; Dorsey, J. G. *J. Chromatogr., A* **2000**, *877*, 41.

(9) Stalcup, A. M.; Martire, D. E.; Wise, S. H. *J. Chromatogr.* **1988**, *442*, 1.

(10) Matteoli, E.; Lepori, L. *J. Chem. Phys.* **1984**, *80*, 2856.

(11) Marcus, Y. *J. Chem. Soc., Faraday Trans. 1* **1989**, *85*, 381.

(12) Marcus, Y.; Migron, Y. *J. Phys. Chem.* **1991**, *95*, 400.

(13) Henry, M. C.; Wolf, L. K.; Messmer, M. C. *J. Phys. Chem. B* **2003**, *107*, 2765.

(14) (a) Martini, G.; Ottaviani, M. F.; Romanelli, M. *J. Colloid Interface Sci.* **1983**, *94*, 107. (b) Romanelli, M.; Ottaviani, M. F.; Martini, G. *J. Colloid Interface Sci.* **1983**, *96*, 373. (c) Martini, G.; Bindi, M.; Ottaviani, M. F.; Romanelli, M. *J. Colloid Interface Sci.* **1985**, *107*, 140, 108. (d) Martini, G.; Ottaviani, M. F.; Romanelli, M.; Kevan, L. *Colloid Surf.* **1989**, *41*, 149.

(15) (a) Ottaviani, M. F.; Mollo, L.; Fubini, B. *J. Colloid Interface Sci.* **1997**, *191*, 154. (b) Ottaviani, M. F.; Tomatis, M.; Fubini, B. *J. Colloid Interface Sci.* **2000**, *224*, 169.

(16) Moscatelli, A.; Galarneau, A.; Di Renzo, F.; Ottaviani, M. F. *J. Phys. Chem. B* **2004**, *108*, 18580.

(17) Liu, Z.; Ottaviani, M. F.; Abrams, L.; Lei, X.; Turro, N. J. *J. Phys. Chem. A* **2004**, *108*, 8040.

(18) Ottaviani, M. F.; Turro, N. J.; Jockusch, S.; Tomalia, D. A. *J. Phys. Chem. B* **2003**, *107*, 2046.

(19) (a) Schneider, D. J.; Freed, J. H. In *Biological Magnetic Resonance. Spin Labeling. Theory and Applications*; Berliner, L. J., Reuben, J., Eds.; Plenum Press: New York, 1989; Vol. 8, p 1. (b) Budil, D. E.; Lee, S.; Saxena, S.; Freed, J. H. *J. Magn. Reson. A* **1996**, *120*, 155.